Langmuir

Article

pubs.acs.org/Langmuir

Cationic Poly(*N*-isopropylacrylamide) Block Copolymer Adsorption Investigated by Dual Polarization Interferometry and Lattice Mean–Field Theory

Alexander Shovsky,[†] Stefan Knohl,[‡] Andra Dedinaite,[†,§] Kaizheng Zhu,[∥] Anna-Lena Kjøniksen,[∥,⊥] Bo Nyström,[∥] Per Linse,*[,#] and Per M. Claesson[†,§]

[†]Department of Chemistry, Surface and Corrosion Science, School of Chemical Science and Engineering, KTH Royal Institute of Technology, Drottning Kristinas väg 51, SE-100 44 Stockholm, Sweden

[‡]Physical Chemistry, Faculty of Natural Science, Institute of Chemistry, Chemnitz University of Technology, Strasse der Nationen 62, 09111 Chemnitz, Germany

[§]Institute for Surface Chemistry, P.O. Box 5607, SE-114 86, Stockholm, Sweden

[∥]Department of Chemistry, University of Oslo, P.O. Box 1033, Blindern, N-0315, Oslo, Norway

[⊥]Department of Pharmacy, School of Pharmacy, University of Oslo, P.O. Box 1068, Blindern, N-0316, Oslo, Norway

[#]Physical Chemistry, Department of Chemistry, Lund University, Box 124, SE-221 00 Lund, Sweden

ABSTRACT: A series of cationic diblock copolymers, poly(*N*-isopropylacrylamide)$_{48}$-*block*-poly((3-acrylamidopropyl)trimethylammonium chloride)$_X$, abbreviated as PNIPAAM$_{48}$-*b*-PAMPTMA^+_X (X = 0, 6, 10, 14, and 20), has been synthesized, and their adsorption onto silicon oxynitride from aqueous solution has been investigated using dual polarization interferometry. The polymer adsorption was modeled by using a lattice mean-field theory, and a satisfactory consistency between theory and experiments was found in terms of surface excess and layer thickness. Both theory and experiments show that the adsorption is limited by steric repulsion for $X < X_{max}$ and by electrostatic interactions for $X > X_{max}$. Modeling demonstrates that significant surface charge regulation occurs due to adsorption. Both the nonionic and cationic block exhibit nonelectrostatic affinity to silicon oxynitride and thus contribute to the driving force for adsorption, and modeling is used for clarifying how changes in the nonelectrostatic affinity affects the surface excess. The segments of the nonionic and cationic blocks seem less segregated when both have a nonelectrostatic affinity for the surface compared to the case where the segments had no surface affinity. Adsorption kinetics was investigated experimentally. Two kinetic regimes were observed: the adsorption rate is initially controlled by the mass transfer rate to the surface and at higher coverage is limited by the attachment rate.

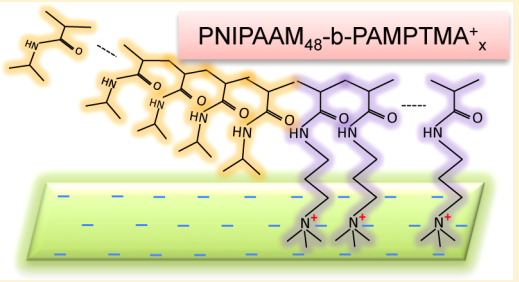

1. INTRODUCTION

Bulk and interfacial properties of diblock copolymers have been extensively studied over the past few decades.[1] Such materials have the capacity to self-organize into association complexes of different geometries when placed in selective solvents, offering great promise for the construction of delivery vehicles and complex nanoscale assemblies.[2,3] Further, charged diblock copolymers are considered to be very efficient agents for colloidal stabilization.[4] In these applications, the charged block interacts strongly with the oppositely charged solid and provides strong anchoring for the buoy block, which, when in a good solvent, provides steric stabilization.[5] Both the length of the anchor block and the length of the buoy block affect surface excess, layer structure, and steric stabilization.

Adsorption kinetics studies provide essential information on the polymer adsorption mechanism,[6] and such aspects are of importance for many industrial processes where the adsorption time is limited.[7] Polymer adsorption kinetics of various polymers on different surfaces has attracted a great deal of interest in the past 2 decades.[8−11] More recently, Cohen Stuart and co-workers described polyvinylamine adsorption kinetics onto cellulose,[12] and Bijelic et al. elucidated the adsorption kinetics of charged bottle-brush polymers on silicon oxynitride.[13] All these studies have demonstrated two adsorption regimes: (i) at low surface coverage the adsorption is transport-limited and (ii) at higher surface coverage a potential barrier created by adsorbed polymers limits the adsorption rate.

Experimental investigations of nonionic-charged diblock copolymers at surfaces have also been performed.[14] For instance, Thomas et al. used a nonpolar block to anchor the charged block to hydrophobized silica and elucidated pH-induced conformational changes in the extended polyelec-

Received: May 29, 2012
Revised: August 27, 2012
Published: August 31, 2012

trolyte buoy block,[15] and Tirrell et al. investigated nonpolar−ionic diblock copolymers adsorbed on hydrophobized mica.[16] The adsorption of diblock copolymers with a nonpolar block and a cationic block on silica has also been considered, and a strong pH-dependence was observed and suggested to be caused by micelle formation on the surface, in analogue to the micellization observed in bulk solution.[17] Furthermore, the case with a diblock copolymer adsorbing primarily via a cationic anchor block and having an uncharged block with less surface affinity was studied recently with emphasis on the temperature dependence of surface forces and friction.[18] In addition, ionic−ionic diblock copolymers have been investigated, and their adsorption properties have been compared with that from mixtures of the two corresponding homopolyelectrolytes.[19]

The adsorption kinetics of diblock copolymers has been considered in some cases. For instance, kinetics of adsorption from diblock copolymer micellar solutions has been investigated.[20,21] Walter et al. investigated adsorption kinetics for ampholytic diblock copolymers and found a strong dependence on the charge ratio of the two blocks as controlled by solution pH.[22] Further, quite intriguing adsorption kinetics were noted for the hydrophobic−anionic diblock copolymer poly(*tert*-butylmethacrylate)-*block*-poly(glycidylmethacrylate sodium sulfonate) on hydrophobic surfaces.[23,24] Three distinct stages in the adsorption process were revealed: an incubation period, a subsequent fast growth process of the polymer layer, and the equilibrium region. In contrast, the kinetics of adsorption for poly(*tert*-butylstyrene)-*block*-poly(sodium styrenesulfonate) on silica surfaces in aqueous solutions has been shown to follow the typical two-stage process where the adsorption rate initially is diffusion-limited but significantly slower at high surface coverage.[25]

Poly(*N*-isopropylacrylamide) (PNIPAAM) is one of the most studied temperature-responsive polymers.[26] In aqueous solution, it exhibits a lower critical solution temperature (LCST) around 32 °C.[27] The phase transition of PNIPAAM is understood to occur as a result of dehydration of the polymer chains at increasing temperature, where destabilization of hydrogen bonds between amide groups of PNIPAAM and water molecules has been implied as one important reason for the dehydration.[26] Interfacial properties of nanometer thick PNIPAAM films on planar and spherical surfaces have attracted scientific attention, partly driven by potential applications in pharmaceuticals and biomedical industries.[28] Several recent reports describe PNIPAAM thin film[29,30] and brush[31] properties.

Surface and solution properties of PNIPAAM can be conveniently tuned by combining PNIPAAM with different polymers in block copolymer structures. For example, thermoresponsive PNIPAAM copolymers have been incorporated in polyelectrolyte multilayers.[30,32] Adsorption properties of a series of cationic block-copolymers $(PNIPAAM)_N$-*b*-$(PNIPAAM)_K$-$(APTAC)_I)_M$ have been studied as a function of charge density on silica and in polyelectrolyte multilayers by quartz crystal microbalance with dissipation monitoring (QCM-D).[30] The surface excess of the diblock copolymers was found to decrease as the charge density of the diblock copolymer increased, and it was suggested that the charged block adsorbed to cellulose with PNIPAAM being non-adsorbing and protruding into solution. Quite recently, Dedinaite et al. described the adsorption properties of $PNIPAAM_{48}$ and cationic $PNIPAAM_{48}$-*b*-$PAMPTMA^+_{20}$ on silica by using QCM-D and reflectometry.[18] It was demonstrated that the homopolymer $PNIPAAM_{48}$ exhibited affinity for silica, whereas adsorption of $PNIPAAM_{48}$-*b*-$PAMPTMA^+_{20}$ on silica was driven by both electrostatics and nonelectrostatic forces.

In this contribution, we consider a series of well-defined charged diblock copolymers poly(*N*-isopropylacrylamide)$_{48}$-*block*-poly((3-acrylamidopropyl)trimethylammonium chloride)$_X$, abbreviated as $PNIPAAM_{48}$-*b*-$PAMPTMA^+_X$, where X has a value between 0 and 20 for the different polymers considered. We examine how the number of monomers of the charged block at constant number of uncharged monomers influences (i) surface excess, (ii) layer structure, and (iii) adsorption kinetics. The experimental work was conducted using dual polarization interferometry (DPI), and silicon oxynitride surfaces. In addition, theoretical modeling utilizing a lattice mean-field theory complemented the experiments. Finally, adsorption kinetics was also investigated experimentally.

2. EXPERIMENTAL SECTION

2.1. Materials. *2.1.1. Polymers.* *N*-Isopropylacrylamide (NIPAAM) (Acros Organics) was recrystallized from toluene/hexane and dried under vacuum prior to use. The homopolymer $PNIPAAM_{48}$ and the cationic diblock copolymers $PNIPAAM_{48}$-*b*-$PAMPTMA^+_X$ with X = 6, 10, 14, or 20 were synthesized following the procedure reported earlier,[18] utilizing atom transfer radical polymerization.[33,34] The chemical structure of the diblock copolymers used in this study is illustrated in Figure 1a. The measured values of the molecular weights M_n and M_w, polydispersity index (M_w/M_n), and refractive index increment (dn/dc) values for these polymers are reported in Table 1.

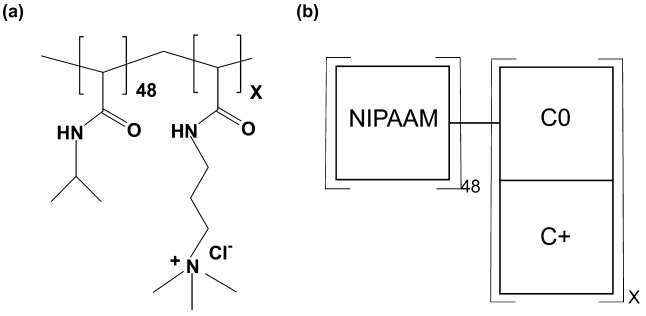

Figure 1. (a) Schematic illustration of the molecular structure of poly(*N*-isopropylacrylamide)$_{48}$-*block*-poly((3-acrylamidopropyl)-trimethylammonium chloride)$_X$ ($PNIPAAM_{48}$-*b*-$PAMPTMA^+_X$) and (b) the coarse-grained model of the cationic diblock polymer where segments C0 and C+ jointly represent $AMPTMA^+$ with segment C+ possessing a positive charge.

2.1.2. Substrate. The substrate surface is a sandwich-like chip structure of two horizontally stacked waveguides made of silicon oxynitride, i.e., nitrogen-doped silica (unmodified Anachip Plus from Farfield Sensors Ltd., Manchester, UK). Prior to measurements, the chip surface was cleaned by using the following steps: (i) dipping in a (1:1) mixture of HCl (37%) and CH_3OH (abs) for 15 min, (ii) rinsing with water, (iii) dipping in 2% surfactant-free Deconex 20 NS (Fisher Scientific) for 15 min, (iv) rinsing with water, and (v) storing in water for 12 h. The chip surface was additionally cleaned by injection of a surfactant-free solution of Deconex 20 NS (2%) for 20 min, followed by rinsing with water until stable DPI signals were achieved (30 min).

2.1.3. Sample Preparation. The water used in all experiments was first pretreated with a Milli-RO 10 Plus unit and then further purified with a Milli-Q PLUS 185 system. The resistivity after the treatment was 18.2 MΩ cm, and the total organic carbon content of the water did not exceed 2 ppb. Stock solutions of the diblock copolymers with a

dx.doi.org/10.1021/la302154p | *Langmuir* 2012, 28, 14028−14038

Table 1. Some Characteristics of $PNIPAAM_{48}$-*b*-$PAMPTMA_X$

	M_n (g/mol)			
X^a	NMR[b]	AFFFF[c]	M_w/M_n (AFFFF)[c]	dn/dc^d (mL/g)
0	5500	4730	1.13	0.163
6	6770	7800	1.05	0.161
10	7600	8100	1.07	0.163
14	8420	8700	1.05	0.164
20	9690	10300	1.05	0.156

[a]Number of charged monomers in the cationic block. [b]Calculated from the ratio of the integral values of the characteristic proton peaks of the different blocks (NIPAAM and AMPTMA) with the end group (ethylpropionate) of the initiator (ethyl 2-chloropropionate) from their ^{1}H NMR spectra. [c]Determined by asymmetric flow field-flow fractionation (AFFFF) employing an AF2000 FOCUS system from Postnova Analytics (Landsberg, Germany) using 1 wt % solutions in 0.01 M NaCl ($X \leq 6$) or 0.1 M NaCl ($X \geq 10$) at a flow rate of 0.2 mL/min and a regenerated cellulose membrane with a cutoff of 1000. More details about the AFFFF measurements can be found in ref 18. [d]Determined by the refractive index detector of the AFFFF instrument.

concentration of 500−1000 ppm were prepared in water by vigorously stirring for ≈24 h followed by filtering using 0.1 μm inorganic membrane filters (Whatman, Anotop 25). Diblock copolymer solutions with a concentration of 50 ppm were prepared by dilution of the corresponding stock solution using purified water. The sample preparation was performed at room temperature.

2.2. Methods. *2.2.1. Dual-Polarization Interferometry.* Dual-polarization interferometry allows measurements of both thickness and refractive index of adsorbed layers in situ and in real time. An AnaLight Bio200 DPI instrument from Farfield Sensors Ltd. (Manchester, UK) was used, and it consists of (i) a helium−neon laser with emitted light at 632.8 nm, (ii) a means to select plane-polarized light, (iii) a sensor constructed by using two optical waveguides stacked one on the top of the other, and (iv) a camera. A detailed description of the instrument is provided by Swann et al.[35]

Briefly, plane-polarized laser light enters the short end of the surface, where it splits and travels separately through the two waveguides (sensing and reference). The two waves interfere with each other as they emerge from the waveguide, and a camera in the far field detects the resulting fringe pattern. The evanescent field emitted into solution in the sensing waveguide is affected by changes in the index of refraction of the bulk solution and by adsorption onto the surface. Hence, the light propagating through the sensing waveguide is somewhat changed relative to the light traveling through the reference waveguide. This difference is detected as a shift in the fringe pattern in the far field, and these shifts are alternately and continuously recorded for both horizontally and vertically polarized light.

A 100 μm thick silicon mask with two slits is placed on top of the waveguide chip. These two slits create two separate flow channels that constitute the actual measurement chambers. Solution is continuously flowed through the channels by use of a syringe pump (model PHD200, Harvard Apparatus), and samples are injected through an HPLC valve and can be directed to flow through both or one of the two channels. Before the adsorption experiment is started, the instrument and the waveguide are calibrated by injecting two solutions of known index of refraction, in this case degassed water and ethanol (80%). Degassed water was also used as rinsing buffer. The flow rate was 50 μL/min, and measurements were performed at 25 °C.

For a homogeneous and isotropic adsorption layer, the thickness, d_f, and the refractive index, n_f, of the adsorption layer can uniquely be calculated from the measured DPI signals.[36] The surface excess, Γ, of the layer is thereafter calculated through

$$\Gamma = \frac{d_f(n_f - n_{buffer})}{\frac{dn}{dc}} \quad (1)$$

2.2.2. Flow Conditions and Mass Transfer. The fluidic system of the AnaLight Bio200 DPI instrument is comprised of (i) a Rheodyne HPLC injector valve, (ii) an external pump (MilliGAT, Global FIA), and (iii) a DPI microfluidic flow chamber. The fluidic system facilitates controlled continuous flow of polymer solution over the chip.[37] The volume of the DPI flow cell used in this study is 1.96 μL, and with a flow rate of 50 μL/min, it takes around 2.4 s to introduce the solution over the entire chip surface. The described flow cell and flow rate parameters ensure a parabolic laminar flow profile throughout the experiment.

The DPI microfluidic flow chamber is designed after the biosensor thin layer cell described by Glaser[38] with well-characterized mass-transfer characteristics. The analytical solution for mass transport to the surface is given by[38,39]

$$j = k(c_b - c_s) \quad (2)$$

where j denotes the flux of polymer from the bulk to the surface, c_b the polymer concentration of the injected solution, and c_s the concentration of nonadsorbed polymers adjacent to the surface, and k is the transport coefficient given by

$$k = 0.98\left(\frac{D_{app}{}^2F}{h^2wl}\right)^{1/3} = 1.26 \times 10^{-7}D_{app}{}^{2/3} \quad (3)$$

where the prefactor for the cell used was determined by Glaser,[38] D_{app} is the apparent diffusion constant, F is the volumetric flow rate, and h = 0.2 mm is the height, w = 0.7 mm is the width, and l = 14 mm is the length of the flow cell. Since all measurements were conducted under the same flow conditions, the results from different experiments are directly comparable in terms of material supply to the surface, enabling us to evaluate adsorption kinetics following the procedure described by Dijt et al.[9]

2.2.3. Electrokinetic Analyzer. The ζ-potential for planar silicon oxynitride surfaces was determined using an electrokinetic analyzer (Anton Paar GmbH, Graz, Austria), a technique that has been described in detail.[40,41] Briefly, an electrolyte solution is flowed across a channel formed by two identical plates. The generated pressure difference and a streaming current (as well as streaming potential) are measured.[42] In our studies, we used two rectangular slides of silicon oxynitride with size 10 mm × 8 mm mounted parallel to each other and separated by a 100 ± 5 μm gap in the measuring cell. For smooth surfaces and laminar flow the Helmholtz−Smoluchowski approach can be applied to calculate the ζ-potential) according to[40,41]

$$\zeta = \frac{I_s}{\Delta P}\frac{\lambda\eta}{\varepsilon\varepsilon_0}\frac{L}{H} \quad (4)$$

where ε is the dielectric constant of the solvent, ε_0 the permittivity of vacuum, η the viscosity of the medium, I_s the streaming current, ΔP the pressure difference, and λ the specific electric conductivity of the electrolyte solution in the channel, and L and H are the channel length and widths, respectively.

3. THEORETICAL MODEL

The adsorption of the cationic diblock copolymers onto a planar and negatively charged surface was modeled on the basis of a lattice mean-field theory, initially developed by Scheutjens and Fleer[40,41] and later extended to polyelectrolytes (see, e.g., ref 42 and references given therein). For the sake of briefness, we will here only give the main features of the theory; for more details, we refer the reader to the original publications.

Briefly, the space adjacent to a planar surface is divided into layers, and each layer is further divided into lattice cells of equal size. Within each layer the Bragg−Williams approximation of random mixing is applied, and thus all sites in a given layer are equivalent. One lattice cell contains either (i) solvent, (ii) a polymer segment, (iii) a solvated cation, or (iv) a solvated anion. The polymer is composed of two blocks: one linear with

dx.doi.org/10.1021/la302154p | Langmuir 2012, 28, 14028−14038

$r_{PNIPAAM}$ = 48 segments representing PNIPAAM and one with $r_{PAMPTMA}$ = 0−40 segments representing PAMPTMA. The latter block possesses $X = r_{PAMPTMA}/2$ main-chain segments (labeled C0), where each have one side-chain composed of one segment carrying a positive charge (labeled C+). Figure 1b illustrates the model of $PNIPAAM_{48}$-*b*-$PAMPTMA^{+}_{X}$. The cationic diblock copolymer is considered to be flexible. The surface is modeled as having a fixed surface potential ψ_s.

There are two different types of interactions in the model: electrostatic (charge−charge) and nonelectrostatic (the rest) ones. The nonelectrostatic interaction between species in adjacent lattice sites is described by Flory−Huggins χ-parameters.[43] The same description is used for the interaction with the surface. Since only the differences of the interaction parameters involving a surface are relevant, we introduce $\Delta\chi_\alpha = \chi_{\alpha,surface} - \chi_{solvent,surface}$, α being a polymer segment (NIPAAM, C0, or C+). The relation to the adsorption parameter χ_s is given, e.g., for the polymer by $\chi_s = -\lambda_{1,0}\Delta\chi_{polymer}$, $\lambda_{1,0}$ being the fraction of all neighbors of a site in layer 1, which resides in the surface layer. Here, $\lambda_{1,0}$ = 1/4, since a hexagonal lattice was selected. The lattice topology only affects the λ matrix, and the outcome of the model is only mildly affected by the choice of lattice topology.[44]

In line with the random mixing approximation, charged species (charged polymer segments and salt species) are assumed to interact with a potential of mean force, ψ_i, which depends only on the distance to the surface (layer number i). Thus, ion−ion correlation effects are not considered in this type of theoretical model. The potential of mean force is related to the charge density through Poisson's equation, $-\varepsilon_0\varepsilon_r\nabla^2\psi_i = \rho_i$, where $\varepsilon_0\varepsilon_r$ is the dielectric permittivity of the medium and ρ_i is the total charge density in layer i. The charges of the species are located to planes in the middle of each lattice layer, and the space in between the charged planes is free of charge. A uniform dielectric permittivity equal to that of water is used.

From the set of volume fraction profiles of the species, $\{\phi_{Ai}\}$, and the interaction parameters, a nonelectrostatic potential u_{Ai} can be calculated for species A in layer i. There is also a layer-dependent but species-independent hard-core potential, u'_i, acting on each species. This potential is essentially the lateral pressure and is responsible for making the volume fraction in each layer sum up to 1. Given the electrostatic energy $q_A\psi_i$ and the nonelectrostatic energy u_{Ai} of species A in layer i as well as the hard-core potential energy u'_i of a segment layer i, the distribution of *unconnected* segments of type A is given by the Boltzmann weight of the sum of the three terms, $\phi_{Ai} \sim \exp\{-(q_A\psi_i + u_{Ai} + u'_i)/kT\}$. For polymers, the matter becomes more complex since the connectivity has to be taken into account. Finally, since $\{\phi_{Ai}\}$ depends on $\{u_{Ai}\}$ and $\{\psi_i\}$, and $\{u_{Ai}\}$ and $\{\psi_i\}$ are functions of $\{\phi_{Ai}\}$ as indicated above, $\{\phi_{Ai}\}$, $\{u_{Ai}\}$, and $\{\psi_i\}$ have to be solved self-consistently. A numerical solution of this set of implicit and nonlinear equations was carried out using up to 80 layers.

Parameters used in the model calculations of the adsorption of $PNIPAAM_{48}$-*b*-$PAMPTMA^{+}_{X}$ cationic diblock copolymers onto silicon−oxynitride surface are compiled in Table 2. Some of the parameters (T, ε_r, $r_{PNIPAAM}$, $r_{PAMPTMA}$, $\phi_{polymer} \equiv \phi_{PNIPAAM} + (\phi_{C0} + \phi_{C+})$, and $\phi_{salt} \equiv \phi_+ + \phi_-$) are known characteristics of the experimental systems. The values of some other parameters (d_l and ψ_s) are less obvious, and some reasonable assignments were used. Here, we have adopted the lattice cell length l_{cell} = 0.5 nm and the surface potential ψ_s = −0.14 V (see also Discussion). Finally, we have the remaining parameters:

Table 2. Model Parameters[a]

quantity	value
temperature	T = 300 K
relative dielectric permittivity	ε_r = 80
lattice spacing	d_l = 0.5 nm
degree of polymerization (PNIPAAM)	$r_{PNIPAAM}$ = 48
degree of polymerization (PAMPTMA)	$X = r_{PAMPTMA}/2$ = 0−20
bulk polymer volume fraction	$\phi_{polymer} = 1 \times 10^{-4}$
bulk salt volume fraction	$\phi_+ = \phi_- = 1 \times 10^{-4}$
surface potential	ψ_s = −0.14 V
interaction parameters[b]	$\chi_{polymer,water}$ = 0.5
	$\Delta\chi_{polymer}$ = −4
conversion factors[c]	Γ_{exp} (mg/m^2) = 2.7 Γ_{exe}
	C_{salt} (M) = 13.3 ϕ_{salt}

[a]Values of model parameters if nothing else is stated. [b]Other interaction parameters are zero. [c]Obtained from the size of a lattice cell and molecular molar mass.

$\chi_{NIPAAM,solvent}$, $\chi_{AMPTMA,solvent}$, $\Delta\chi_{NIPAAM}$, and $\Delta\chi_{AMPTMA}$ (with AMPTMA denoting both C0 an C+). First, for simplicity we assigned $\chi_{NIPAAM,solvent} = \chi_{AMPTMA,solvent} \equiv \chi_{polymer,solvent}$ and $\Delta\chi_{PNIPAAM} = \Delta\chi_{AMPTMA} \equiv \Delta\chi_{polymer}$. Temporarily disregarding the charge of the AMPTMA monomer, both monomers are considered to have similar hydrophobicity when viewing their chemical structure. Furthermore, we adopted $\chi_{polymer,solvent}$ = 0.5 as being a reasonable value, understanding that the adsorption is only weakly sensitive to it, and $\Delta\chi_{polymer}$ = −4, which was essentially fitted but is still reasonable. Experimentally, it is known that PNIPAAM at 300 K displays a weak hydrophobic character (which is more pronounced at elevated temperature) and adsorbs onto silica-like surfaces.[18]

On the basis of the volume fraction profiles $\{\phi_{Ai}\}$, the surface excess of a diblock copolymer Γ_{exe} is given by

$$\Gamma_{exe} = \sum_i \phi_{polymer,i} - \phi_{polymer,bulk} \tag{5}$$

and the thickness of the adsorbed polymer layer d was evaluated through[44]

$$d = \frac{\left[\sum_i (\phi_{polymer,i} - \phi_{polymer,bulk})\right]^2}{\sum_i (\phi_{polymer,i} - \phi_{polymer,bulk})^2} \tag{6}$$

where both quantities are given in units of the lattice length l_{cell}.

4. RESULTS

4.1. Adsorption of the $PNIPAAM_{48}$ Homopolymer and $PNIPAAM_{48}$-*b*-$PAMPTMA^{+}_{X}$ Block Copolymers. The time evolution of the surface excess and layer thickness during adsorption of $PNIPAAM_{48}$ and of $PNIPAAM_{48}$-*b*-$PAMPTMA^{+}_{X}$ on silicon oxynitride from water are provided in Figures 2 and 3, respectively. Initially, the surface excess increases linearly with time, and then the adsorption rate decreases as surface saturation is approached. At equilibrium, for the chosen bulk polymer concentration, the surface excess of $PNIPAAM_{48}$ is 0.6 mg/m^2 and the layer thickness is 1.4 nm. This demonstrates that PNIPAAM exhibits affinity to the silicon oxynitride surface and adsorbs via nonelectrostatic interactions.

At a bulk polymer concentration of 50 ppm, the surface excess found for $PNIPAAM_{48}$ and the different diblock copolymers in the plateau region are displayed in Figure 4. When a short cationic block with X = 6 monomers is

dx.doi.org/10.1021/la302154p | Langmuir 2012, 28, 14028−14038

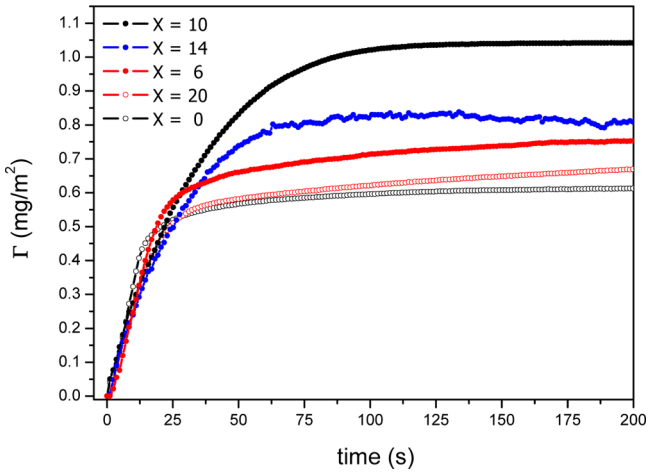

Figure 2. Surface excess of adsorbed PNIPAAM$_{48}$-*b*-PAMPTMA$^{+}{}_{X}$ on silicon oxynitride surface as a function of time at indicated values of *X*. The polymer concentration was 50 ppm.

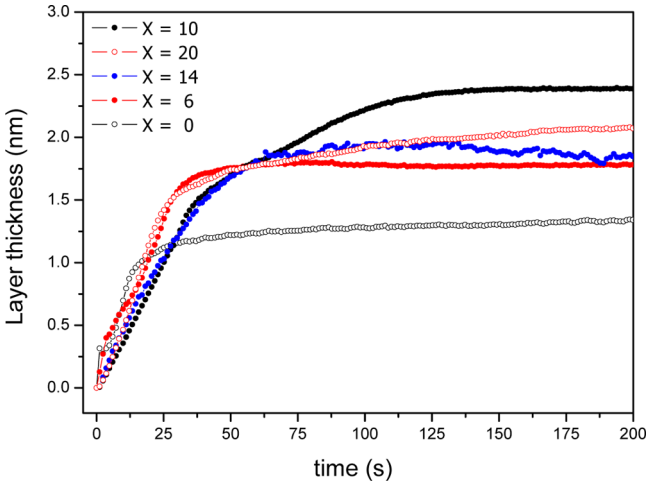

Figure 3. Thickness of adsorbed PNIPAAM$_{48}$-*b*-PAMPTMA$^{+}{}_{X}$ layers on silicon oxynitride as a function of time at indicated values of *X*. The polymer concentration was 50 ppm.

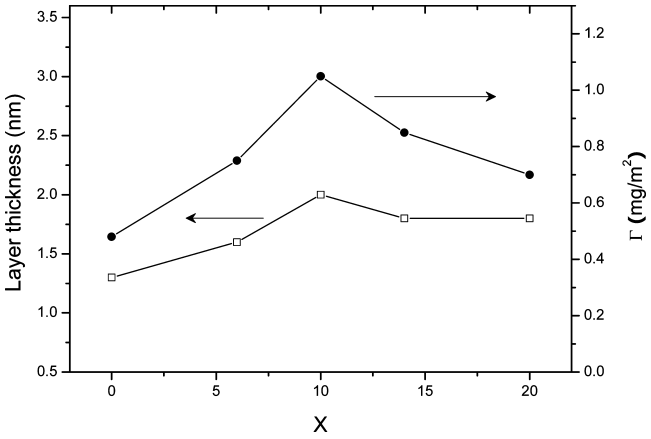

Figure 4. Surface excess (●) and thickness (□) of adsorbed PNIPAAM$_{48}$-*b*-PAMPTMA$^{+}{}_{X}$ layer on silicon oxynitride as a function of the number of charged monomers in the copolymer. The polymer concentration was 50 ppm.

incorporated in the polymer structure, the surface excess increases to 0.8 mg/m^2. A further increase in the length of the cationic block to $X = 10$ increases the surface excess to 1.1 mg/m^2, whereas an even longer cationic block, $X = 20$, results in a decrease of the surface excess down to 0.7 mg/m^2. The variation in layer thickness mimics that of the surface excess in the sense that the maximum value is found for $X = 10$. However, for a similar surface excess a slightly larger thickness is observed for the cationic-rich polymers as compared to the cationic-poor ones. For instance, the surface excess for $X = 6$ is 0.8 mg/m^2, and the layer thickness is 1.6 nm. For diblock copolymers with $X = 14$ and 20, the surface excess is 0.9 and 0.7 mg/m^2, respectively, but in both cases a layer thickness of 1.8 nm is observed.

The surface excess in the plateau region can be recalculated in terms of number of adsorbed polymer charges and number of adsorbed polymers. The results from these calculations are shown in Figure 5. For diblock copolymers with $X \geq 10$, the

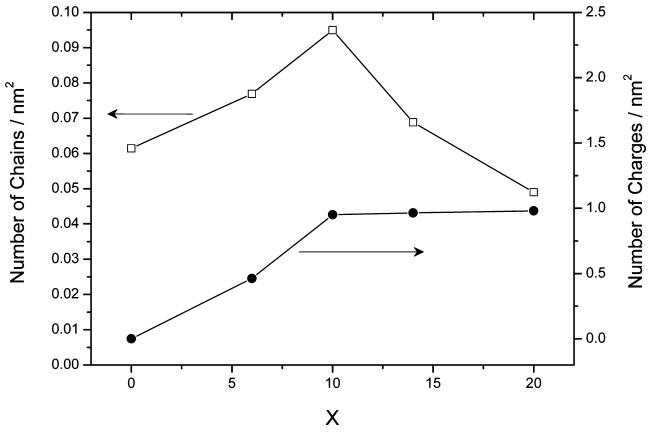

Figure 5. Number of chains (□) and charged monomers (●) per nm^2 of adsorbed PNIPAAM$_{48}$-*b*-PAMPTMA$^{+}{}_{X}$ layer on silicon oxynitride of as a function of the number of charged monomers in the diblock copolymer. The polymer concentration was 50 ppm.

same number of charged groups is adsorbed, which is a strong indication that the adsorption proceeds until the electrostatic repulsion counteracts further adsorption. The number of adsorbed chains is at a maximum value for $X = 10$, whereas the number of adsorbed polymers with $X = 20$ charged monomers is even lower than that found for polymers with no charged monomers, $X = 0$. Again, this is suggested to be a consequence of electrostatic repulsion within the layer.

4.2. Lattice Mean−Field Calculations. Surface excess calculated using the lattice mean-field approach is compared with experimental results in Figure 6. First, we observe that (i) the calculated surface excess, using a reasonable set of parameters, is in magnitude similar to the measured one. Furthermore, in both cases it is noted that (ii) the surface excess goes through a maximum at $X = X_{max}$ as the length of the cationic AMPTMA$^+$ block is increased, (iii) a gentler decrease at $X > X_{max}$ and a sharper one at $X < X_{max}$, and (iv) the dependence on X is stronger in theory. Experimentally the maximum in the surface excess is observed for $X = X_{exp}^{max} = 10$, whereas modeling predicts a maximum at a smaller value of the degree of polymerization of the cationic block, viz. $X = X_{theory}^{max} = 4$.

We note that for $X > X_{max}$ electrostatic interactions control the surface excess (Figures 5 and 6), whereas for $X < X_{max}$ the

dx.doi.org/10.1021/la302154p | *Langmuir* 2012, 28, 14028−14038

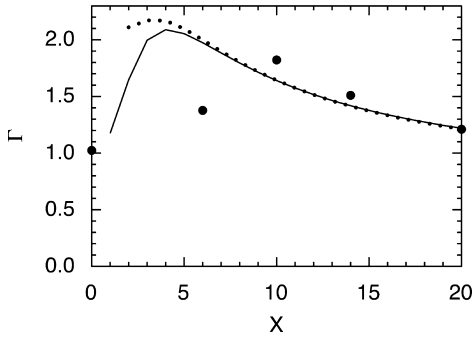

Figure 6. Calculated (solid curve) and experimental (symbols) surface excess as a function of the number of charged monomers in the diblock copolymer. Calculated surface excess, provided the surface charge was perfectly compensated by the charges of the adsorbed polymer, is also shown (dotted curve).

surface excess is dictated by repulsion between the uncharged segments, and in this regime the surface excess increases with the number of charged segments.

Calculated and experimentally determined layer thicknesses are compared in Figure 7. The same four observations made for

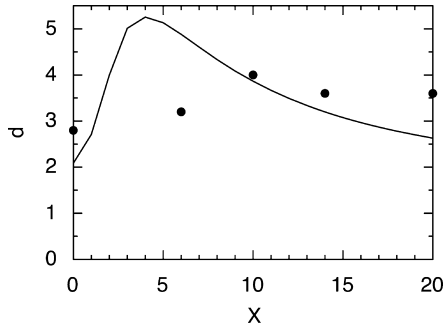

Figure 7. Calculated (curve) and experimental (symbols) thickness of adsorbed polymer layer as a function of the number of charged monomers in the diblock copolymer.

the surface excess prevails for the layer thickness, the main difference being a weaker dependence on X for the experimental data. We note that the experimental "layer thickness" is not a well-defined quantity. In the DPI instrument, it is evaluated by assuming a homogeneous segment density profile across the layer, whereas, as will be illustrated by the modeling results, this is not the case. On the other hand, in the modeling the polymer layer thickness was defined by eq 6, which is considered to be consistent with the layer thickness determined by ellipsometry,[47] which uses a similar "homogeneous layer" model as in the DPI.

The condition of constant surface potential implies a charge regulation, which depends on the distribution of the charged species near the surface. Figure 8a shows that a substantial charge regulation appears in the present system. The charge density of the surface before adsorption of polymers is $\sigma = -0.045$. As the nonionic−cationic diblock copolymer adsorbs, the magnitude of the negative charge density of the surface increases significantly with increasing number of monomers of the cationic block from $\sigma = -0.037$ for $X = 0$ and reaches $\sigma = -0.276$ for $X = 20$. This result is consistent with previous results for linear[45] and bottle-brush polyelectrolytes.[46] We also note that adsorption of the nonionic block alone ($X = 0$) results in a small decrease in the magnitude of the surface charge

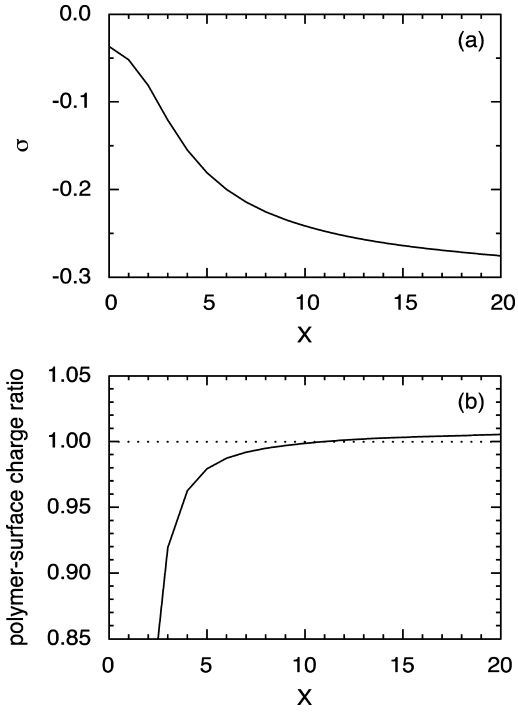

Figure 8. Calculated (a) surface charge density in the presence of adsorbed polymer layer and (b) ratio between the charge density arising from adsorbed polymers and the surface charge density as a function of number of charged monomers in the diblock copolymer.

density. This is a consequence of depletion of small salt ions from the immediate proximity of the surface by the polymer.

The degree to which the surface charge density is neutralized by the adsorbed diblock copolymer is illustrated in Figure 8b. We note that already for such a small cationic block as $X = 4$, the surface charge neutralization factor of the adsorbed polymer is close to 0.96. As X increases, the degree of neutralization increases further and reaches close to unity for $X = 11$. A further increase to $X = 20$ results in a small overcharging, where the ratio between polymer charges and surface charges is 1.0058. The relatively small variation in surface charge density and close to perfect charge compensation predicted for large values of X imply that the predicted numbers of charged segments are close to independent of X in this region. This is also observed in the experimental results for $X \geq 10$ (see Figure 5).

The segment density profile is not accessible with the DPI technique used for evaluating the adsorption. However, this quantity is directly obtained from the lattice mean-field calculations. The results for some selected block structures are shown in Figure 9a. The uncharged polymer block, $X = 0$, shows the most rapid decay in segment density away from the surface, which explains why the layer thickness for this polymer is the smallest. The calculations show that copolymer with $X = 4$ displayed the most extended layer of all polymers investigated, and this is related to this copolymer giving the highest surface excess in the calculations (cf. Figure 6). For the copolymer with the largest cationic block, $X = 20$, we note a small depletion starting in layer 15. This is a consequence of the slight overcompensation of the surface charge density for this copolymer (Figure 8b).

It is also of interest to consider the segment density distribution for the two blocks separately. Such data are shown

dx.doi.org/10.1021/la302154p | *Langmuir* 2012, 28, 14028−14038

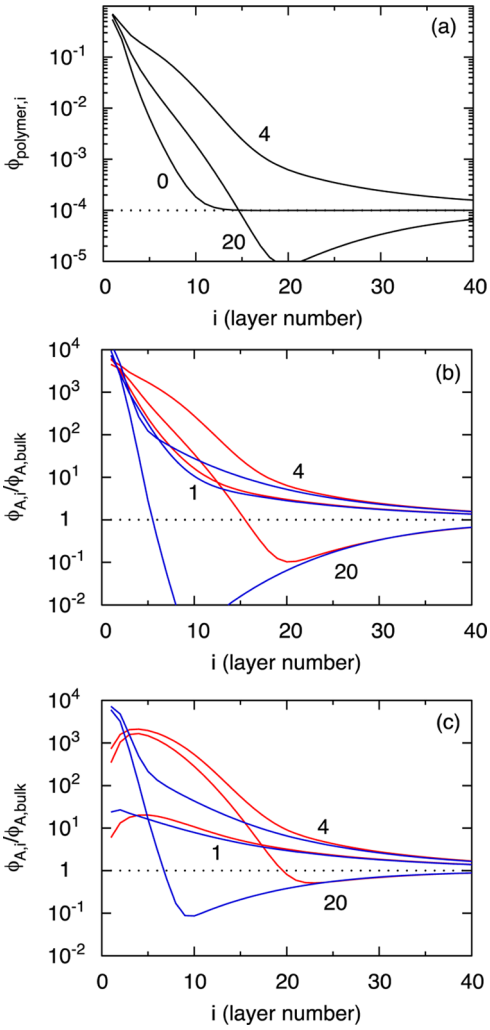

Figure 9. Calculated (a) polymer density, (b) accumulation factor (segment density/segment density in bulk) for PNIPAAM (red) and PAMPTMA (blue), and (c) accumulation factor for PNIPAAM (red) and PAMPTMA (blue) for the situation with *no* polymer-surface nonelectrostatic affinity as a function of the distance from the surface at indicated values of X.

in Figure 9b in terms of accumulation factor expressing the relative volume fraction with respect to that in bulk. First, we note that both blocks are strongly accumulated in the first layer, $i = 1$, in agreement with both having affinity for the surface. The accumulation factor in the first layer is larger for the segments in the cationic block than for those in the nonionic block. This is caused by the electrostatic attraction between the cationic segments and the surface. However, for $i \geq 2$ the accumulation factor is larger for the nonionic block, but the accumulation factor for the charged segments remains significantly larger than unity also in several layers away from the surface. For comparison, the segment density profiles for the two blocks were also calculated for the case with no affinity between the polymer segments and the surface ($\Delta\chi_{polymer} = 0$), and the results are illustrated in Figure 9c. By comparing the data presented in parts b and c of Figure 9, we note as expected that the accumulation factor for PNIPAAM in the absence of nonelectrostatic affinity is less close to the surface, and the segment density for this block reaches a maximum a few layers away from the surface. The PNIPAAM block is also observed to extend further away from the surface in the absence of the nonelectrostatic surface affinity. The importance of the nonelectrostatic affinity increases with decreasing size of the cationic block. This is clearly shown for the case with $X = 1$, where the accumulation factor is much larger when a nonelectrostatic attraction is present. We also note that the depletion layer is less pronounced for the diblock copolymer with $X = 20$, which is a consequence of a decreasing overcharging of the surface. In general, we find that the degree of overcharging under conditions where the electrostatics limits the adsorption increases with increasing nonelectrostatic affinity (e.g., for $X = 20$ from 1.0007 at $\Delta\chi_{polymer} = 0$ to 1.0056 at $\Delta\chi_{polymer} = -4$).

4.3. Adsorption Kinetics. A common feature of the surface excess vs time curves illustrated in Figure 2 is that the surface excess initially increases linearly with time. This is as expected for a diffusion-limited adsorption process.[47] (Note that data for the first 200 s are shown in Figure 2, whereas the equilibrium surface excess after about 10 min is shown in Figure 4). The initial adsorption rate is similar for all of the polymers investigated, but the time required to saturate the surface is slightly larger for the diblock copolymers, PNIPAAM$_{48}$-*b*-PAMPTMA$^{+}_{X}$, compared to for the homopolymer PNIPAAM$_{48}$. This indicates that rearrangements in the layer occur more slowly for the diblock copolyelectrolytes.

When mass transport determines the initial adsorption rate, it becomes

$$\left(\frac{d\Gamma}{dt}\right)_0 = k_{exp}c_b \tag{7}$$

($c_s = 0$ in eq 2),[47] and the numerical values for k_{exp} are provided in Table 3. We note that if all polymers that arrive to the surface also adsorb, then $k_{exp} = k$ in eq 2, but a lower value may be obtained, if, for example, not all orientations of the polymer lead to adsorption. In our case, we expect the value of k_{exp} to be very similar to that of k, since both blocks have affinity for the surface. In the initial adsorption regime, differences in adsorption rates are related only to differences in polymer diffusion constants and proportional to $D^{2/3}$. Qualitatively, one would expect the diffusion constant to decrease somewhat as the size of the charged block is increased. This is the general trend observed, but the scatter of the data is too large to allow us to draw any firm conclusions.

Table 3. Mass Transport Coefficients for PNIPAAM$_{48}$-*b*-PAMPTMA$_X$

X^a	$k_{exp}{}^b$ (10^{-7} m s^{-1})
0	7.2
6	6.3
10	6.2
14	6.0
20	6.4

[a]Number of charged monomers in the cationic block. [b]The uncertainties in these values are about ±5%.

It is possible to analyze the kinetic curves, $\Gamma(t)$, further in terms of transport of molecules and their attachment rates. The attachment rate, or the apparent adsorption rate, $d\Gamma/dt$, depends on the concentration of free polymer molecules close to the surface c_s, as shown in eq 2 according to

$$\frac{d\Gamma}{dt} = K(\Gamma)c_s \tag{8}$$

dx.doi.org/10.1021/la302154p | *Langmuir* 2012, 28, 14028−14038

where $K(\Gamma)$ is the attachment rate constant that depends on the surface excess Γ. Using eqs 3, 7, and 8, the attachment rate constant can be extracted from[47]

$$\frac{1}{K(\Gamma)} = c_b\left(\frac{1}{\frac{d\Gamma}{dt}} - \frac{1}{k_{exp}}\right) = c_b\left(\frac{1}{\frac{d\Gamma}{dt}} - \frac{1}{\left(\frac{d\Gamma}{dt}\right)_0}\right) \quad (9)$$

The relative importance of mass transport and attachment rate can be assessed by comparing the observed initial adsorption rate coefficient k_{exp} and the attachment rate constant $K(\Gamma)$. Some results are shown in Figure 10. We note that as long as the surface excess is less than about 0.4 mg/m^2 the difference between $(d\Gamma/dt)_0$ and $d\Gamma/dt$ is too small to allow a determination of $K(\Gamma)$, and close to the plateau value the noise becomes large. Nevertheless, in the region following the mass transport limiting stage, the attachment rate constant decreases rapidly and roughly exponentially with increasing surface excess (Figure 10). A similar exponential dependence has been observed for the adsorption kinetics of bottle-brush polyelectrolytes.[13] This strong reduction in adsorption rate is due to the steric hindrance imposed by the already adsorbed polymers. In the case where charge reversal occurs, electrostatic interactions also slow down adsorption due to development of a depletion layer.

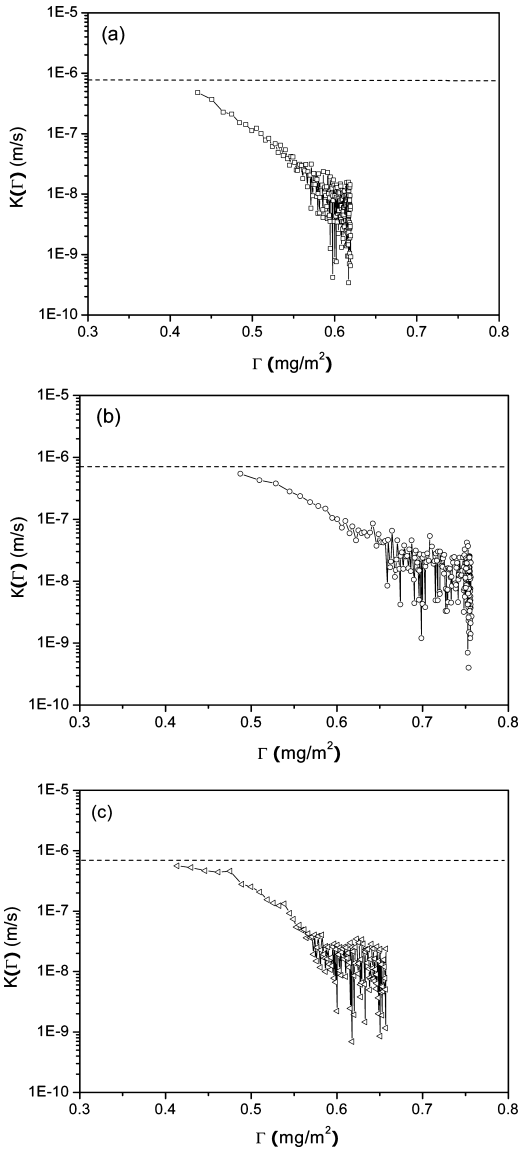

Figure 10. Attachment rate constant (logarithmic scale) $K(\Gamma)$ (points) and observed initial adsorption rate coefficient k_{exp} (dotted line) for adsorption of PNIPAAM$_{48}$-*b*-PAMPTMA^+_X on silicon oxynitride surface as a function of surface excess for (a) $X = 0$, (b) $X = 6$, and (c) $X = 20$ charged monomers in the diblock copolymer. The polymer concentration was 50 ppm.

5. DISCUSSION

5.1. Adsorption of Homopolymers on Silicon Oxynitride. Silicon oxynitride has an isoelectric point at pH 3, and the ζ-potential at pH 6 is about −50 mV in 1 mM KCl, as determined by us using streaming potential measurements. It is similar, but not identical, to silica. It has previously been shown that PNIPAAM adsorbs to glass[48] and silica[18] surfaces, and thus, it is not surprising that adsorption occurs also to silicon oxynitride. The surface excess of PNIPAAM$_{48}$ on silica has been found to be 0.3 mg/m^2 at pH 6, as determined by optical reflectometry. Thus, PNIPAAM$_{48}$ adsorbs in larger amounts on silicon oxynitride (0.6 mg/m^2) as compared to silica. The higher refractive index of silicon oxynitride (about 1.5) compared to silica (1.45−1.46) will affect the van der Waals attraction between the surface and the polymer, and one may speculate that this influences the surface excess. However, also other factors like the surface density and type of silanol groups may differ and affect the surface excess.

In dilute solutions with no added salt, it is generally accepted that highly charged polyelectrolytes adopt stretched conformations due to electrostatic repulsion between the segments.[52] Adsorption studies of polyelectrolytes with similar molecular structure to PAMPTMA^+_X have been reported on silicon oxynitride,[13] silica,[49] and mica.[50] In all cases, as long as the ionic strength is low, the highly charged polyelectrolytes have been found to adsorb in flat conformations, resulting in low surface excess and very thin adsorbed layers. This is also confirmed by Monte Carlo simulations[51] and by the lattice mean-field calculations presented here and in previous work.[45] This is due to the strong electrostatic surface affinity.

5.2. Structure of PNIPAAM$_{48}$-*b*-PAMPTMA^+_X Copolymer Layers. The traditional picture of an adsorbed layer of a diblock copolymer comprises that the anchor block appears in close proximity to the surface and the buoy block extends out into solution.[36] This situation is approached if the buoy block experiences sufficiently good solvency conditions and has no affinity for the surface. An alternative scenario is that the copolymer forms micelles at the surface. However, we have no indications of that at low temperature as PNIPAAM molecules repel each other. As a consequence, the lateral mean-field approximation of the copolymer distribution in the theory should be satisfactory.

The theoretically determined segment distributions for the two blocks for diblock copolymers with $X = 1$, 4, and 20 under these conditions are depicted in Figure 9c. The results of the lattice mean-field model show that the presence of a nonelectrostatic affinity between the two blocks and the surface (as in the experimental system) has a pronounced influence of the segment density profile and results in a larger accumulation factor for segments of both blocks at the surface than would be expected for a nonadsorbing nonionic block (cf. Figure 9b and c). Hence, the mixing of segments of the two blocks becomes

dx.doi.org/10.1021/la302154p | *Langmuir* 2012, 28, 14028−14038

larger when both blocks display a nonelectrostatic surface affinity.

The maximum number of cationic segments was brought to the surface by the diblock copolymer with the largest cationic block (X = 20) as determined both experimentally and by theory. However, the difference between X = 10 and 20 was small, since electrostatics limits the adsorption to that needed to (closely) balance the charges of the charge regulating surface, and variation of the surface charge density is limited between X = 10 and 20 (Figure 8a). The maximum amount of NIPAAM segments on the surface was found for the composition $X = X_{max}$, where the theoretical determined maximum was found to be at a lower value X_{max} = 4 than experimentally obtained X_{max} = 10. Thus, it seems that the highest amount of NIPAAM segments in the adsorbed layer is achieved for a block copolymer composition at the border between the regimes where electrostatics and steric interactions limit the adsorption.

The nonelectrostatic surface affinity has a strong influence on the surface excess, independent of the block copolymer structure. This is illustrated in Figure 11a. Without any nonelectrostatic surface affinity, no adsorption occurs for the uncharged block due to entropic repulsion. However, some adsorption occurs for X = 2, and then adsorption increases rapidly and reaches a maximum for X = 5. Adding a nonelectrostatic affinity for the nonionic block increases the adsorption significantly at low X, but has only a limited effect for X > 5. Adding a nonelectrostatic affinity also to the cationic block increases the surface excess further for all values of X > 0. The X-value that gives maximum adsorption decreases when a nonelectrostatic affinity is present (cf. dotted and full curves in Figure 11a), but the shift is rather small.

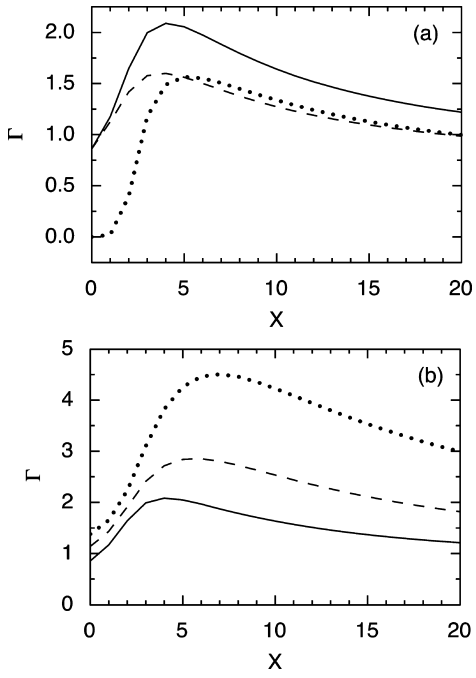

Figure 11. Calculated surface excess as a function of the number of charged monomers in the diblock copolymer for (a) ($\Delta\chi_{NIPAAM}$, $\Delta\chi_{AMPTMA}$) = (−4, −4) (solid curve), (−4, 0) (dashed curve), and (0,0) (dotted curve) and (b) r_{NIPAAM} = 48 (solid curve), 100 (dashed curve), and 200 (dotted curve) PNIPAAM segments.

The calculated data in Figure 11b illustrates how the surface excess depends on the size of the nonionic block, $r_{PNIPAAM}$. For all values of X, a longer nonionic block results in larger surface excess, and the maximum increases to larger values of X (X = 4 for $r_{PNIPAAM}$ = 48 to X = 7 for $r_{PNIPAAM}$ = 200). This is a consequence of increased steric repulsion between the adsorbed nonionic chains. Moreover, at small X (e.g., X = 4) the volume fraction of cationic segments in the first layer *increases* with increasing $r_{PNIPAAM}$, whereas at larger X (e.g., X = 10) the volume fraction of cationic segments in the first layer *decreases* with increasing $r_{PNIPAAM}$. In the former regime, the volume fraction of cationic segments is relatively low, enabling the number of adsorbed copolymers to increase, whereas in the other regime the volume fraction of cationic segments is higher, making the number of adsorbed copolymers decrease, at increasing $r_{PNIPAAM}$.

Finally, the seemingly large discrepancy in experimental and theoretical values of X_{max} is puzzling, and we have no reasonable explanation for it. This discrepancy relies only on one experimental data point, viz., at X = 6. However, we have not been able to trace any error in the experimental procedure of this composition that could explain this discrepancy. The approximate treatment of the charge−charge correlation is less likely a reason, as that should affect the comparison more gradually across the different values of X. Nevertheless, our aim with the modeling was not to fit the experimental data in detail, rather to have a model that reasonably describes the experimental observations and then analyze the role of different parameters on various properties to improve our understanding of the experimental system.

6. SUMMARY

The adsorption of a series of well-defined and relatively short cationic diblock copolymers, $PNIPAAM_{48}$-*b*-$PAMPTMA^{+}_{X}$ ($0 \leq X \leq 20$), on silicon oxynitride substrates has been investigated by dual polarization interferometry, and the experimental results have been compared to predictions based on a lattice mean-field theory. Satisfactory agreement between experimental results and theoretical predictions were obtained with reasonable choices of the interaction parameters. Both the uncharged PNIPAAM block and the cationic $PAMPTMA^{+}$ block were found to have a nonelectrostatic affinity for the surface. The surface excess and thickness of the adsorbed polymer layers were quantitatively determined and found to depend on the length of the cationic block. A maximum of both these quantities was found to occur for the polymer composition X = 10, which is larger than the X = 4 predicted by the theory. For shorter cationic blocks, the adsorption was limited by the repulsion between the adsorbed PNIPAAM blocks, whereas for longer cationic blocks the adsorption was limited by electrostatic repulsion. This conclusion is supported by the close to constant amount of cationic groups associated with the surface for compositions with $X \geq X_{max}$, as also predicted by the modeling.

The modeling provides a detailed understanding of the adsorption process. It demonstrates the importance of surface charge regulation, particularly for longer cationic blocks, where the ability of the surface to regulate its charge density enhances the surface excess. Modeling also predicts that the present situation, where both the nonionic block and the cationic block has nonelectrostatic affinity to the surface, results in a rather different adsorbed layer structure compared to the case with no such surface affinity. The nonelectrostatic surface affinity (i) increases the accumulation factor at the surface for segments in both blocks, (ii) decreases the layer thickness, and (iii)

dx.doi.org/10.1021/la302154p | *Langmuir* 2012, 28, 14028−14038

decreases the degree of segregation between the two blocks away from the surface. The model calculations also predict that an increased length of the nonionic block results in increased surface excess and shifts the value of X that results in maximum surface excess to a larger number.

The initial adsorption rate was found to be close to independent of block copolymer composition, and the mass transport to the surface is the rate-determining process in the initial adsorption stage for all polymers studied. This first stage involves diffusion of the copolymer chains to the solid surface, followed by rapid attachment. This situation prevails until the surface coverage reaches 0.3−0.4 mg/m^2, after which the adsorption kinetics slows down significantly due to restrictions imposed by already adsorbed polymers, with an exponential decrease in attachment rate with increasing surface excess.

AUTHOR INFORMATION

Corresponding Author

*E-mail: per.linse@fkem1.lu.se.

Notes

The authors declare no competing financial interest.

ACKNOWLEDGMENTS

This work was financed by the Norwegian Research Council (Grant No. 1777665/V50 and 190403) (B.N.), by VINNOVA through a VINNMER grant (Grant No. P38574-1) (A.D.), the Swedish Research Council (VR) through the Linnaeus Center of Excellence Organizing Molecular Matter (Grant No. 239-2009-6794) (P.L.) and a project grant (Grant No. 621-2011-3309) (P.C.), and by EU through the NanoS3 project (Grant No. 290251) of the FP7-PEOPLE-2011-ITN call.

REFERENCES

(1) Netz, R. R.; Joanny, J.-F. Adsorption of semiflexible polyelectrolytes on charged planar surfaces: Charge compensation, charge reversal, and multilayer formation. *Macromolecules* **1999**, *32*, 9013−9025.

(2) Hales, K.; Pochan, D. J. Using polyelectrolyte block copolymers to tune nanostructure assembly. *Curr. Opin. Colloid Interface Sci.* **2006**, *11*, 330−336.

(3) Rodriguez-Hernandez, J.; Checot, F.; Gnanou, Y.; Lecommandoux, S. Toward 'smart' nano-objects by self-assembly of block copolymers in solution. *Prog. Polym. Sci.* **2005**, *30*, 691−724.

(4) Cohen Stuart, M. A.; Hofs, B.; Voets, I. K.; de Kaizer, A. Assembly of polyelectrolyte-containing block copolymers in aqueous media. *Curr. Opin. Colloid Interface Sci.* **2005**, *10*, 30−36.

(5) Bijsterbosch, B. H.; Cohen Stuart, M. A.; Fleer, G. J. Effect of block and graft copolymers on the stability of colloidal silica. *J. Colloid Interface Sci.* **1999**, *210*, 37.

(6) Huguenard, C.; Pefferkorn, E. Rate of adsorption of diblock copolymers from micellar solutions on solid−liquid interfaces. *Macromolecules* **1994**, *27*, 5271−5276.

(7) Wittmer, J.; Joanny, J.-F. Charged diblock copolymers at interfaces. *Macromolecules* **1993**, *26*, 2691−2697.

(8) Motschmann, H.; Stamm, M.; Toprakcioglu, C. Adsorption kinetics of block copolymers from a good solvent: A two-stage process. *Macromolecules* **1991**, *24*, 3681−3688.

(9) Dijt, C. J.; Cohen Stuart, M. A.; Hofman, J. E.; Fleer, G. J. Kinetics of polymer adsorption in stagnation point flow. *Colloids Surf.* **1990**, *51*, 141−158.

(10) Dijt, J. C.; Cohen Stuart, M. A.; Fleer, G. J. *Adv. Colloid Interface Sci.* **1994**, *50*, 79−101.

(11) Hoogeveen, N. G.; Cohen Stuart, M. A.; Fleer, G. J. Polyelectrolyte adsorption on oxides. I. Kinetics and adsorbed amounts. *J. Colloid Interface Sci.* **1996**, *182*, 133−145.

(12) Geffroy, C.; Labeau, M. P.; Wong, K.; Cabane, B.; Cohen Stuart, M. A. Kinetics of adsorption of polyvinylamine onto cellulose. *Colloids Surf. A* **2000**, *172*, 47−56.

(13) Bijelic, G.; Shovsky, A.; Varga, I.; Makuska, R.; Claesson, P. M. Adsorption characteristics of brush polyelectrolytes on silicon oxynitride revealed by dual polarization interferometry. *J. Colloid Interface Sci.* **2010**, *348*, 189−197.

(14) Toomey, R.; Mays, J.; Tirrell, M. In situ thickness determination of adsorbed layers of poly(2-vinylpyridine)-polystyrene diblock copolymers by ellipsometry. *Macromolecules* **2004**, *37*, 905−911.

(15) An, S. W.; Thirtle, P. N.; Thomas, R. K.; Baines, F. L.; Billingham, N. C.; Armes, S. P.; Penfold, J. Structure of a diblock copolymer adsorbed at the hydrophobic solid/aqueous interface: Effects of charge density on a weak polyelectrolyte. *Macromolecules* **1999**, *32*, 2731−2738.

(16) Balastre, M.; Li, F.; Schorr, P.; Yang, J.; Mays, J. W.; Tirrell, M. V. A study of polyelectrolyte brushes formed from adsorption of amphiphilic diblock copolymers using the surface forces apparatus. *Macromolecules* **2002**, *35*, 9480−9486.

(17) Strykas, D. A.; Bütün, V.; Lu, J. R.; Keddie, J. L.; Armes, S. P. pH-controlled adsorption of polyelectrolyte diblock copolymers at the solid/liquid interface. *Langmuir* **2000**, *16*, 5980−5986.

(18) Dedinaite, A.; Thormann, E.; Olanya, G.; Claesson, P. M.; Nyström, B.; Kjøniksen, A.-L.; Zhu, K. Friction in aqueous media tuned by temperature-responsive polymer layers. *Soft Matter* **2010**, *6*, 2489−2498.

(19) Mahltig, B.; Gohy, J.-F.; Jerome, R.; Buchhammer, H.-M.; Stamm, M. Analogy in adsorption behavior of homopolyelectrolyte mixtures as compared to analogous diblock polyampholytes. *J. Polymer Sci. B* **2002**, *40*, 338−345.

(20) Bijsterbosch, B. H.; Cohen Stuart, M. A.; Fleer, G. J. Adsorption kinetics of diblock copolymers from a micellar solution on silica and titania. *Macromolecules* **1998**, *31*, 9281−9294.

(21) Toomey, R.; Mays, J.; Tirrell, M. The role of salt in governing the adsorption mechanism of micelle-forming polyelectrolyte/neutral diblock copolymers. *Macromolecules* **2006**, *39*, 697−702.

(22) Walter, H.; Harrats, C.; Müller-Buschbaum, P.; Jerome, R.; Stamm, M. Adsorption of ampholytic diblock copolymers from dilute aqueous solutions at the solid/liquid interface. *Langmuir* **1999**, *15*, 1260−1267.

(23) Abraham, T.; Giasson, S.; Gohy, J.-F.; Jerome, R.; Müller, B.; Stamm, M. Adsorption kinetics of a hydrophobic−hydrophilic diblock polyelectrolyte at the solid-aqueous solution interface: A slow birth and fast growth. *Macromolecules* **2000**, *33*, 6051−6059.

(24) Abraham, T. Effects of divalent salt on adsorption kinetics of a hydrophobically modified polyelectrolyte at the neutral surface−aqueous solution interface. *Polymer* **2002**, *43*, 849−855.

(25) Amiel, C.; Sikka, M.; J.W., S.; Tsao, Y.-H.; Tirrell, M.; Mays, J. W. Adsorption of hydrophilic−hydrophobic block copolymers on silica from aqueous solutions. *Macromolecules* **1995**, *28*, 3125−3134.

(26) Schild, H. G. Poly(*N*-isopropylacrylamide): Experiment, theory and applications. *Prog. Polym. Sci.* **1992**, *17*, 163−249.

(27) Kubota, K.; Fujishige, S.; Ando, I. Single-chain transition of poly(*N*-isopropylacrylamide) in water. *J. Phys. Chem.* **1990**, *94*, 5154−5158.

(28) Liu, S.; Maheshwari, R.; Kiick, K. L. Polymer-based therapeutics. *Macromolecules* **2009**, *42*, 3−13.

(29) Motornov, M.; Roiter, Y.; Tokarev, I.; Minko, S. Stimuli-responsive nanoparticles, nanogels, and capsules for integrated multifunctional intelligent systems. *Prog. Polym. Sci.* **2010**, *35*, 174−211.

(30) Utsel, S.; Malmström, E.; Carlmark, A.; Wågberg, L. Thermoresponsive nanocomposites from multilayers of nanofibrillated cellulose and specially designed *N*-isopropylacrylamide based polymers. *Soft Matter* **2010**, *6*, 342−352.

(31) Zhang, J.; Nylander, T.; Campbell, R.; Rennie, A.; Zauscher, S.; Linse, P. Novel evaluation method of neutron reflectivity data applied to stimulus-responsive brushes. *Soft Matter* **2008**, *4*, 500−509.

(32) Quinn, A.; Such, G. K.; Quinn, J. F.; Caruso, F. Polyelectrolyte blend multilayers: A versatile route to engineering interfaces and films. *Adv. Funct. Mater.* **2008**, *18*, 17−26.
(33) Matyjaszewski, K.; Xia, J. Atom transfer radical polymerization. *Chem. Rev.* **2001**, *101*, 2921−2990.
(34) Tsarevsky, N. V.; Matyjaszewski, K. "Green" atom transfer radical polymerization: From process design to preparation of well-defined environmentally friendly polymeric materials. *Chem. Rev.* **2007**, *107*, 2270−2299.
(35) Swann, M. J.; Peel, L. L.; Carrington, S.; Freeman, N. J. Dual-polarization interferometry: An analytical technique to measure changes in protein structure in real time, to determine the stoichiometry of binding events, and to differentiate between specific and nonspecific interactions. *Anal. Biochem.* **2004**, *329*, 190−198.
(36) Cross, G. H.; Reeves, A.; Brand, S.; Swann, M. J.; Peel, L. L.; Freeman, N. J.; Lu, J. R. The metrics of surface adsorbed small molecules on the Young's fringe dual-slab waveguide interferometer. *J. Phys D* **2004**, *37*, 74−80.
(37) Karim, K.; Taylor, J. D.; Cullen, D. C.; Swann, M. J.; Freeman, N. J. Measurement of conformational changes in the structure of transglutaminase on binding calcium ions using optical evanescent dual polarisation interferometry. *Anal. Chem.* **2007**, *79*, 3023−3031.
(38) Glaser, R. W. Antigen−antibody binding and mass transport by convection and diffusion to a surface: A two-dimensional computer model of binding and dissociation kinetics. *Anal. Biochem.* **1993**, *213*, 152−161.
(39) Sjölander, S.; Urbaniczky, C. Integrated fluid handling system for biomolecular interaction analysis. *Anal. Chem.* **1991**, *63*, 2338−2345.
(40) Scheutjens, J. M. H. M.; Fleer, G. J. Statistical theory of the adsorption of interacting chain molecules. 1. Partition function, segment density distribution, and adsorption isotherms. *J. Phys. Chem.* **1979**, *83*, 1619−1635.
(41) Fleer, G. J.; Cohen Stuart, M. A.; Scheutjens, J. M. H. M.; Cosgrove, T.; Vincent, B. *Polymers at Interfaces*; Chapman & Hall: London, 1993.
(42) Linse, P. Adsorption of weakly charged polyelectrolytes at oppositely charged surfaces. *Macromolecules* **1996**, *29*, 326−336.
(43) Flory, P. J. *Principles of Polymer Chemistry*; Cornell University Press: Ithaca, NY, 1953.
(44) McCrackin, F. L.; Colson, J. P. In *Ellipsometry in the Measurements of Surfaces and Thin Films*; Passaglia, E., Stromberg, R. R., Kruger, J., Eds.; National Bureau Standards Miscellaneous Publications: Washington, DC, 1964; p 61.
(45) Shubin, V.; Linse, P. Self-consistent-field modeling of polyelectrolyte adsorption on charge-regulating surfaces. *Macromolecules* **1997**, *30*, 5944−5952.
(46) Linse, P.; Claesson, P. M. Modeling of bottle-brush polymer adsorption onto mica and silica surfaces. *Macromolecules* **2009**, *42*, 6310−6318.
(47) Dijt, C. J.; Cohen Stuart, M. A.; Fleer, G. J. Competitive adsorption kinetics of polymers differing in length only. *Macromolecules* **1994**, *27*, 3219−3228.
(48) Callewaert, M.; Grandfils, C.; Boulangé-Petermann, L.; Rouxhet, P. G. Adsorption of poly(*N*-isopropylacrylamide) on glass substrata. *J. Colloid Interface Sci.* **2004**, *276*, 299−305.
(49) Olanya, G.; Iruthayaraj, J.; Poptoshev, E.; Makuska, R.; Vareikis, A.; Claesson, P. M. Adsorption characteristics of bottle-brush polymers on silica: Effect of side chain and charge density. *Langmuir* **2008**, *24*, 5341−5349.
(50) Dahlgren, M. A. G.; Claesson, P. M.; Audebert, R. Highly charged cationic polyelectrolytes on mica: Influence of polyelectrolyte concentration on surface forces. *J. Colloid Interface Sci.* **1994**, *166*, 343−349.
(51) Dahlgren, M. A. G.; Waltermo, Å.; Blomberg, E.; Claesson, P. M.; Sjöström, L.; Åkesson, T.; Jönsson, B. Salt effects on the interaction between adsorbed cationic polyelectrolyte layers—Theory and experiment. *J. Phys. Chem.* **1993**, *97*, 11769−11775.